Supporting Material

Mechanism of Cis-Inhibition of PolyQ Fibrillation by PolyP: PPII Oligomers and the Hydrophobic Effect

Gregory D. Darnell, JohnMark Derryberry, Josh W. Kurutz, and Stephen C. Meredith

Supplementary Information

Peptide Synthesis and Purification

Peptides were synthesized and cleaved essentially as described previously except that amino acids were singly coupled during all syntheses (S1). All reagents were from sources as previously described (S1). In addition, the peptides were highly soluble and did not need to be centrifuged after disaggregation. PolyQ peptides were purified as described previously (S1). For peptides with polyP segments, it was necessary to use isocratic mixtures of water:acetonitrile:TFA (94:6:0.1 to 91:9:0.1, water:acetonitrile:TFA, v:v:v, for various peptides, Burdick Jackson and Halocarbon). PolyP peptides were purified using a preparative Zorbax C_3 reverse phase column. After purification, all peptides were flash frozen and lyophilized.

Peptides were analyzed by electrospray ionization (ESI) and/or MALDI-TOF mass spectrometery. Purity was assessed by analytical HPLC on an Agilent 1100 system equipped with either a Microsorb C_{18} (for polyQ peptides) or Microsorb C_3 (for polyP peptides) analytical reverse phase column, eluted with water:acetonitrile (both with 0.1% TFA, v:v) gradients. Final peptide purity for all peptides was $\geq$ 95%. Lyophilized peptides were stored at -20 °C in sealed glass vials until needed. In some cases, purity and mass were reexamined before and after experiments to ensure no chemical modifications occurred during handling.

Disaggregation Procedure

Although peptides appeared to be soluble without a disaggregation procedure, such a procedure was employed as a way to increase yields of peptide in chromatography steps. Thus, peptides were dissolved in a mixture of neat TFA (200 µL) and neat HFIP (200 µL) in

siliconized Eppendorf tubes and sonicated at room temperature in a Branson 2510 tabletop

sonciator for ten minutes. After sonication, organic solvent was removed by evaporation under

N_2. The dried peptides were then dissolved in buffer or water. In some cases, solutions were

centrifuged at 13,200 rpm at room temperature for five minutes in an Eppendorf 5415D tabletop

centrifuge to remove small amounts of particulate material. The dissagregation procedure did

not chemically modify any of the peptides. Concentration was determined by UV absorbance at

274.6 nm, using a Hitachi U2000 spectrometer and a 1cm quartz cell (Starna), and the extinction

coefficient for free tyrosine in 10mM sodium phosphate at room temperature, $1420 \text{ M}^{-1} \text{ cm}^{-1}$.

For many CD experiments in which precise determination of peptide concentration was

important for calculating mean residue ellipticity, peptide concentration was confirmed by

analytical reverse phase HPLC. Samples were injected onto a C18 column as described above,

and the effluent was monitored by absorbance at 274.6 nm. The mass of peptide in the injected

sample was calculated from the area of the peak using the same extinction coefficient of $1420 \text{ M}^{-1} \text{ cm}^{-1}$.

CD spectra of other variants of short polyQ, polyP and polyQ-polyP peptides show PPII-like helical structure

Circular dichroism was used to characterize the secondary structure of short polyQ,

polyP, and tandem polyQ-polyP tracts. Previous studies have shown that short polyQ peptides

with ≤ nine glutamines adopt a polyproline type II (PPII) conformation in solution (S1-S3). The

addition of a polyP segment to the C-terminal end of the polyQ tract increases the threshold

number of Gln residues required for fibril formation (S4), and may do so by inducing PPII-like

helical structure in the polyQ segment (S1). Supplementary Figure 1 shows that short polyQ

peptides containing only three Gln residues, with or without a tandem polyP tract, also adopt this secondary structure when freshly dissolved and assayed at higher concentrations (455 µM and at 4 °C and neutral pH. The PPII-like structure is shown by positive ellipticity in the 217-230 nm region, indicative of a left-handed helical structure, and negative ellipticity in the 201-216 nm region (S5-S7).

$R_3GP_{11}GY$ contains a polyP segment and no glutamines, and hence is taken as having a *bona fide* PPII helix; it had a maximum positive ellipticity at 229.5 nm. As in our previous paper (S1), the polyQ peptides are considered as having PPII-like helical structure, since the maximal positive ellipticity of these peptides is not the same as that of $R_3GP_{11}GY$, and this may reflect subtle structural differences as well. The spectrum of $R_3GP_{11}GY$ also shows a trough with a minimum at 215 nm. Although a trough at this wavelength is often associated with β-sheet peptides, it is highly unlikely that a covalently constrained polyP peptide would be able to adopt a β-sheet conformation. It is more reasonable to infer that the trough at these wavelengths is also associated with polyprolines in the PPII conformation, as has been reported elsewhere (S5-S7). Comparing R_3GQ_3GY to $R_3GQ_3P_{11}GY$, the addition of the polyP segment makes the CD spectrum of the latter peptide quite similar to that of $R_3GP_{11}GY$, indicating that the polyP tract dominates the spectrum of the tandem peptide. Without a polyP tract, R_3GQ_3GY has a broader and blue-shifted maximum at 217.5 nm, and a shallower trough, with a minimum at 201.5 nm, but this spectrum is also consistent with a left-handed, PPII-like structure. As a control for the flanking residue, we also examined R_3AQ_3AY, which has a CD spectrum similar to that of R_3GQ_3GY, with the same minimum and maximum, although the trough is somewhat deeper. Thus, only minor variations in the spectra occur from changing the linker residue from Gly to Ala.

CD spectra of additional variants of these peptides (Group II) are shown in Supplementary Figure 2. For these peptides, the order of the sequences flanking the polyQ or polyQ-polyP domain is reversed from the above four peptides, i.e., the chromophore, Tyr, is at the N-terminus, and an Arg residue is at the C-terminus. The basic features of these spectra are similar to those shown in Supplementary Figure 1, i.e., there is a peak of positive ellipticity at 220-231 nm and a trough with a minimum at 204-219nm. In general, the latter group of peptides had somewhat red-shifted minima and maxima and approximately two-fold higher Mean Residue Ellipticities.

Supplementary Figure 3 shows the CD spectra of these peptides at pH 3.0 (Supplementary Figure 3A and 3B for Group I and Group II, respectively). In general, for these peptides, lowering the pH to 3.0 yielded similar spectra, except for the fact that all peptides showed significant hyperchromism at pH 3.0. Taken together with the results shown in Supplementary Figures 1 and 2, these data suggest that lower pH tends to stabilize PPII-like helical structure, as do Ala residues flanking the polyQ and polyP segments.

To assess the stability of the CD spectra over time, CD spectra were measured at 0-2 h, two days, one week, and one month after disaggregating and dissolving the peptides. This incubation procedure was performed for four concentrations of each peptide (10, 20-60, 100 and 455 μM). CD spectra were measured at 4 and 25 °C, and peptide solutions were maintained at this temperature between measurements. Peptide concentration was checked only at the beginning time point as no visible aggregates were seen for the duration of the entire experiment. CD signals were collected from 260-190 nm at 4 °C with 0.5 nm step sizes, 1 nm bandwidths, and 1 s averaging times. Spectra are a result of three averaged scans from a representative experiment. Supplementary Figure 4 shows that CD spectra of Group I peptides did not change

over time even at high concentration (455 mM) for periods up to a month. At no time were

insoluble aggregates visible in these solutions. Solutions of Group II peptides showed the

similar stability in CD spectra and size exclusion chromatographs (data not shown).

Thermal "Unfolding" of Peptides

To assess the change in CD spectra of peptides as a function of temperature, peptides

were freshly dissolved, disaggregated, and diluted to 455 or 493 µM in 10 mM sodium

phosphate, at either pH 7.00 or 3.00, to a volume of ~ 500 µl. A 0.1 cm cell was used (Starna)

with a Teflon cap to prevent evaporation. Scans were from 265 to 190 nm with a bandwidth of 1

nm and a stepsize of 1 nm. Averaging time at each wavelength was 1 s. Temperature was

arrayed from 0 to 80 °C with a 5 °C step size and a temperature deadband of 0.1 °C. Three scans

were performed at each temperature, and a pause of two minutes between each temperature

increment was allowed for thermal equilibration. Spectra were measured for both peptide

samples and buffers at each temperature. Heating and cooling curves were measured without a

pause between heating and cooling measurements.

For thermodynamic analysis of melting of the PPII-like helix, we examined a null

hypothesis of a two-state system, using an equation denoting equilibrium between a folded and

an unfolded state. Thus,

$$K_{eq} = \frac{f_u}{f_f} \hspace{6cm} \text{Supp. Eq. 1}$$

where f_u = fraction unfolded, and f_f = fraction folded. These fractions are given by

$$f_u = \frac{\theta_{exp} - \theta_u}{\theta_f - \theta_u}$$

Supp. Eq. 2

and

$$f_f = \frac{\theta_f - \theta_{exp}}{\theta_f - \theta_u}$$

Supp. Eq. 3

where θ_{exp} = experimental ellipticities and θ_f and θ_u are parameters, the ellipticities for the folded and unfolded state, which are obtained by non-linear least squares fit of the data. Thus,

$$K_{eq} = \frac{\theta_{exp} - \theta_u}{\theta_f - \theta_{exp}} = \exp(-\Delta G / RT)$$

Supp. Eq. 4

The effect of temperature on the CD spectra of Group I and Group II peptides is shown in Figure 1 and Supplementary Figure 5, respectively. The results of analyses using Supp. Eq. 4 are shown in Supplementary Figures 6 and 7 for Group I and Group II peptides, respectively. There is only very slight curvature to these lines; most of the curve is outside of the experimentally accessible temperature range. The peptides approach the "unfolded" state only at infinitely high temperatures. This indicates that the null hypothesis was incorrect, and the melting is not indicative of a two-state system. Rather, this behavior demonstrates local unfolding or unraveling of the PPII or PPII-like helices, with loss of left-handedness, possibly to a more extended structure.

Size Exclusion Chromatography

Size exclusion chromatography of previously disaggregated peptides dissolved in 200 mM sodium phophate, pH 7.00 was performed using Superdex 75 or Superdex Peptide columns. Peptides were disaggregated as above, dissolved in 200 mM sodium phosphate, pH 7.00, and the stock was either chromatographed as such or immediately diluted to concentrations ranging from 10-455 μM. Chromatography was performed on 50 μL of peptide solution, using a Superdex 75 column (GE Healthcare), or in more recent experiments, a Superdex Peptide column on an Agilent 1100 series HPLC system equipped with a room temperature auto-sampler. Fresh peptides were injected onto the column with no more than four hours of waiting on the autosampler before injection onto the column. In other experiments, peptides were incubated at 4 °C in siliconized Eppendorf tubes for various times up to one month to mirror the times and conditions of the CD experiments. The column was equilibrated and eluted with 200mM sodium phosphate, pH 7.00. Higher ionic strengths were needed to prevent adsorption of peptide onto the column matrix. Chromatography was performed at room temperature (~ 20 °C), with a flow rate of 0.5 ml/min, and effluent was monitored by UV absorbance at 220, 274.6, or 280 nm. Void and total volumes of the column were determined from the elution positions of dextran (molecular weight 35,000 to 50,000) or bovine serum albumin, and valine, glycine or DMSO, respectively, all from Sigma.

TOCSY and CT-COSY NMR

For NMR spectroscopy, peptides were dissolved after disaggregation, as above, in 200 mM sodium phosphate, at pH 7.0, 5.0, or 1.5-3.0, also containing NaN_3 (0.1%, w:v). A 1.0 mM solution of sodium 2,2-dimethyl-2-silapentane-5-sulfonate (DSS, Cambridge Isotope

Laboratories) was used for external chemical shift referencing at the various temperatures at which two-dimensional NMR spectra were measured (see below). Spectra were measured using 8 inch, 5 mm thin-walled glass NMR tubes (Wilmad-Labglass) with an 800 MHz rating. Solutions were vacuum degassed for 10 minutes in tabletop dessicators, filled with a nitrogen atmosphere, and then capped and sealed with Parafilm to prevent evaporation. NMR samples were stored at 4 °C until needed. The most current version of Biopack software (Varian) was used to set up initial pulse sequence parameters. All data were processed using NMRPipe freeware software (National Institutes of Health) using zero filling and solvent subtraction methods. For suppression of the signal from water, typically eight pre-saturation Watergate pulse sequences were used for each experiment. Automatic shimming of Z1 and Z2 shims were also performed before each experiment.

Additional NMR data on four peptides (R_3GQ_3GY, $R_3GQ_3P_{11}GY$, YAQ_3AR, and $YAQ_3P_{11}AR$) are presented in Supplementary Figures 8 and 9, which show the "fingerprint" region (NH-Cα) regions of TOCSY and CT-COSY spectra of these peptides, respectively.

CT-COSY (Contant Time COrrelation SpectroscopY) spectra were measured for the same four peptides to obtain $^3J_{NH-C\alpha}$ coupling constants at temperatures from 0-40 °C, or in some cases, up to 60 °C in 5 °C increments; measurements at all temperatures were performed twice, once on heating, and once on recooling. For some peptides, the spectral lineshapes at temperatures above 40 °C became very broad at pH 7.0.

The following procedure was used to obtain $^3J_{NH-C\alpha}$ coupling constants. One-dimensional slices of the two-dimensional data set were taken and the intensity data were extracted using a UNIX script. The data were then fitted to an equation for the difference between two Lorentzian functions, i.e.,

$$\text{Intensity} = y = \left(y_{0,1} + 2\frac{A_1}{\pi}\frac{w_1}{4\left(\nu - \nu_{c,1}\right)^2 + w_1^2} \right) - \left(y_{0,2} + 2\frac{A_2}{\pi}\frac{w_2}{4\left(\nu - x_{c,2}\right)^2 + w_2^2} \right) \qquad \text{Supp. Eq. 5}$$

where $y_{0,1}$ and $y_{0,2}$ are y-intercepts of the two Lorentzian functions, w_1 and w_2 are the two widths

of the peaks, ν is the frequency, $\nu_{c,1}$ and $\nu_{c,2}$ are the frequencies at the center of the two peaks,

and A_1 and A_2 are scaling parameters. As is typical for this type of data, the spectra yielded pairs

of peaks, one positive and one negative. From the fit of the data to the above equation using

Kaleidagraph software (v.3.6.2, Synergy software), a series of $^3J_{NH-xC\alpha}$ coupling constants were

obtained, and these were used to calculate torsional (ϕ) angles, using the Karplus relationship

(S8):

$$^3J_{HN-C\alpha} = 6.4\cos^2\Theta - 1.4\cos\Theta + 1.9 \qquad \text{Supp. Eq. 6}$$

where $\Theta = \phi - 60°$. From the values obtained for the ϕ angles, a $^3J_{NH-C\alpha}$ coupling constant of 3-4

Hz is most consistent with an α-helix, and a $^3J_{NH-C\alpha}$ coupling constant > 8 Hz suggests a β-sheet

(S9). As described by Shi and Kallenbach, a $^3J_{NH-C\alpha}$ coupling constant of 5-7 Hz is consistent

with a PPII-like helical structure (S10).

Supplementary Figure 10 shows examples of a non-linear least squares fits of data from

1-D slices of CT-COSY spectra to the above equation of the difference between two Lorentzian

functions for a single Gln residue (Gln 1) for the same four peptides at the same temperature (~ 0

°C).

Supplementary Information on NMR Diffusion Measurements and Calculations

As described in the body of the paper, diffusion of two peptides, R_3GQ_3GY and $R_3GQ_3P_{11}GY$, was estimated diffusion coefficients using pulsed field gradient NMR, comparing the effective hydrodynamic radii of these peptides in solution to that of a protein standard, FN3s. Supplementary Figure 11 shows the same data presented in Figure 5 of the paper, but without normalizing the curves to an initial signal intensity of unity.

This method requires that the solvent and temperature be constant for all samples. Hence, all measurements on the peptides were made using 200 mM sodium phosphate, pH 7.00 as solvent; this entire set of NMR measurements were made at 5 °C, which was chosen because it led to most effective suppression of the water signal. The reference standard was a structurally well-defined protein made from a synthetic construct for the tenth fibronectin type III domain (S11), here called FN3s. An NMR sample of FN3s was kindly provided by Akiko Koide and Shohei Koide, both from the University of Chicago. FN3s is a well-characterized, compact, spheroidal, globular protein with a molecular weight of 9939.23 (S11).

As described briefly in the body of the paper, this method is based on that of Jones et al. (S12), which, in turn, is an application of an NMR method described previously by Gibbs and Johnson (S13). This method uses a pulse-gradient stimulated echo longitudinal encode-decode (PG-SLED) sequence in which all delays are held constant, and in which only the gradient strength, g, is varied. Under these conditions, the signal intensity depends only on g and the diffusion constant, D, according to the equation:

$$I = I_0 \exp(-dg^2)$$

Supp. Eq. 7

where I = signal intensity, I_0 = initial signal intensity, and the observed rate constant, d, is proportionate to the diffusion coefficient. Because the PG-SLED sequence causes spin-lattice relaxation to appear as an exponential decay (S13) in units proportional to time, one obtains:

$$I = I_0 \exp(-kt) \qquad \text{Supp. Eq. 8}$$

where k = rate constant, which is proportional to the diffusion constant, D.

The pulse sequence for these experiments varies gradient strength, from which the signal intensity, I, decays as a function of the square of the gradient strength. The sequence was written so the parameter controlling gradient strength was defined as a delay, d2; this enables the VNMR software on the spectrometer interface to handle the arrayed diffusion data in as T2 relaxation measurement data, from which first-order rate constants were calculated. The pulse sequence converts these d2 "delays", provided in units of sec/mm^2, to DAC units treated by the gradient amplifier in the following manner. For each d2 value, a variable, b1, is calculated; b1 is defined as

$$b1 = \sqrt{\frac{d2}{(bdelta - (gt1/3))}} \qquad \text{Supp. Eq. 9}$$

where bdelta is the duration of the actual diffusion period, in seconds, and gt1 is the duration of each gradient pulse, in seconds. The units of b1 are mm^{-1}. Before b1 can be converted to a DAC value usable by the gradient amplifier, he pulse sequence calculates a conversion factor, calz, in units of Hz/(mm DAC) from a parameter calibrated to the particular gradient hardware used, gcal, which is given in gauss/(cm DAC).

$$calz = gzcal \times \frac{4257.5}{10} \qquad \text{Supp. Eq. 10}$$

The number 4257.5 is in units of Hz/gauss, and is a constant for ^{1}H nuclei analogous to the more familiar MHz/Tesla conversion. The denominator 10 converts cm to mm. The parameter used to specify gradient pulse strength, g1amp, is calculated to yield DAC units (or can be entered as a variable by the spectroscopist). Here, g1amp is calculated as follows:

$$\text{g1amp} = \frac{\text{b1}}{2\pi \times \text{calz} \times \text{gt1}} \qquad \text{Supp. Eq. 11}$$

Thus, a plot of peak intensity versus d2 is essentially the same as a plot of peak intensity versus g1amp^2, after the X-axis units are multiplied by a conversion factor. In Figure 5 of the paper and in Supplementary Figure 11, the x-axis is presented as G^2, in units of T^2/m^2. The parameter, g1amp (DAC) is converted to T/m as follows:

$$G = \text{g1amp(DAC)} \times \text{calz}(\frac{\text{gauss}}{\text{cm} - \text{DAC}}) \times (\frac{1\text{T}}{10^4 \text{gauss}}) \times (\frac{100\text{cm}}{\text{m}}) \qquad \text{Supp. Eq. 12}$$

Thus, d2 values given in the pulse sequence were converted to G^2, which, in the terms of this experiment, can be treated as a time variable, from which can extract a rate constant proportionate to the diffusion coefficient. As mentioned in the body of the text, because all delays in the PG-SLED pulse sequence are held constant, the signal intensity depends on only the gradient strength, g, which is varied, and the diffusion constant. Thus, as stated above, the PG-SLED sequence causes spin-lattice relaxation to appear as an exponential decay (57), and an observed rate constant can be calculated, in units proportional to time (Eq. 1 of the paper).

Supplementary References

S1.   Darnell, G., J. P. R. O. Orgel, R. Pahl, and S. C. Meredith. 2007. J. Mol. Biol. 374: 688-704.

S2.   O'Nuallain, B., A. K. Thakur, A. D. Williams, A. M. Bhattacharyya, S. Chen, G. Thiagarajan, and R. Wetzel. 2006. Meth. Enz. 413: 34-74.

S3.   Elias, H.-G. 2008. Macromolecules, Volume 3, p. 70, Wiley-VCH Verlag GmbH &Co. KGaA, Weinheim.

S4.   Bhattacharyya, A., A. K. Thakur, V. M. Chellgren, G. Thiagarajan, A. D. Williams, B. W. Chellgren, T. P. Creamer, and R. Wetzel. 2006. J. Mol. Biol. 355: 524-535.

S5.   Okabayashi, H., T. Isemura, and S. Sakakibara. 1968. Biopolymers 6: 323-330.

S6.   Tiffany, M. L., and S. Krimm. 1968. Biopolymers 6: 1767-1770.

S7.   Dukor, R. K., and T. A. Keiderling. 1991. Biopolymers 31: 1747-1761.

S8.   Karplus, M. 1959. J. Phys. Chem. 30: 11-15.

S9.   Wuthrich, K. 1986. NMR of Proteins and Nucleic Acids" pp. 1-292, Wiley, New York.

S10.   Shi, Z., C. A. Olson, G. D. Rose, R. L. and N. R. Kallenbach. 2002. Proc. Natl. Acad. Sci. USA. 99: 9190-9195.

S11.   Koide, A., C. W. Bailey, X. Huang, and S. Koide. 1998. J. Mol. Biol. 284: 1141-1151.

S12.   Jones, J. A., D. K. Wilkins, L. J. Smith and C. M. Dobson. 1997. J. Biomolecular NMR 10: 199–203.

S13.   Gibbs, S. J., and C. S. Johnson Jr. 1991. J. Magn. Reson. 93: 395-402.

Supplementary Figures Legends

1. CD spectra of freshly dissolved and disaggregated polyQ, polyP, and polyQ-polyP peptides at 455 μM, 10 mM sodium phosphate, pH 7.00, 4 °C. Symbols: (λ), R_3GQ_3GY; (ν), $R_3GQ_3P_{11}GY$; (σ), $R_3GP_{11}GY$; and (τ), R_3AQ_3AY.

2. CD spectra of Group II polyQ, polyP, and polyQ-polyP peptides at 455 μM in 10 mM sodium phosphate, pH 7.00, 4 °C. Symbols: (λ), YAQ_3AR; (ν), $YAQ_3P_{11}AR$; (σ), $YAP_{11}AR$; and (τ), YGQ_3GR.

3. Comparison of CD spectra of both Group I and Group II polyQ, polyP, and polyQ-polyP peptides at pH 7.0 and 3.0. Peptides are at 455 μM and in 10 mM sodium phosphate, pH 7.00 at 4 °C. Symbols for Group I: (A): (λ, ○), R_3GQ_3GY, pH 7.0 and 3.0 respectively; (ν, □), $R_3GQ_3P_{11}GY$, pH 7.0 and 3.0 respectively; (σ, △), $R_3GP_{11}GY$, pH 7.0 and 3.0 respectively; and (τ), R_3AQ_3AY, pH 7.0. Symbols for Group II: (B): (▼, ▽), YAQ_3AR, pH 7.0 and 3.0 respectively; (ν, □) $YAQ_3P_{11}AR$, pH 7.0 and 3.0 respectively; and (σ, △), $YAP_{11}AR$, pH 7.0 and 3.0 respectively.

4. Stability of Group I CD spectra over time from freshly dissolved solutions at 455 μM (t = 0 h) in 10 mM sodium phosphate, pH 7.00, and after two days, one week, and one month of incubation at 4 °C. (A), R_3GQ_3GY; (B), $R_3GQ_3P_{11}GY$; (C), $R_3GP_{11}GY$; and (D) R_3AQ_3AY.

5. Thermal melting of Group II polyQ, polyP, and polyQ-polyP peptides. (A), (B), and (C) show CD spectra of YAQ_3AR, $YAQ_3P_{11}AR$, and $YAP_{11}AR$, respectively, at temperatures from 0 to 80 °C, at intervals of 5 °C at 10mM sodium phosphate, pH 7.00. For clarity, only the curves for heating of samples are shown; the curves obtained from cooling samples are essentially super-imposable on those of heating.

6. Analysis thermal melting of Group I polyQ, polyP, and polyQ-polyP peptides. (A), (B), (C), and (D) show Mean Residue Ellipticities at 229 nm of R_3GQ_3GY, $R_3GQ_3P_{11}GY$, $R_3GP_{11}GY$, and R_3AQ_3AY, respectively, as a function of temperature. The figures show experimental data as points, and non-linear least squares fit of the data to the Supp. Eq. 4 as a solid line.

7. Analysis of thermal melting of Group II polyQ, polyP, and polyQ-polyP peptides. (A), (B), and (C) show Mean Residue Ellipticities of of YAQ_3AR, $YAQ_3P_{11}AR$, and $YAP_{11}AR$, respectively, at 229 nm as a function of temperature. The figures show experimental data as points, and non-linear least squares fit of the data to the Supp. Eq. 4 as a solid line.

8. "Fingerprint" region (NH-Cα) regions of TOCSY spectra of polyQ and polyQ-polyP peptides. TOCSY spectra were measured at temperatures at 0, 25, and 50 °C, to make chemical shift assignments. In all cases, peptides were in the mM concentration range, and solvent was 200 mM sodium phosphate, pH 7.00 (with 0.1 % NaN_3, w:v). The figure shows samples of TOCSY spectra measured at 0 °C for (A), R_3GQ_3GY; (B), $R_3GQ_3P_{11}GY$; (C), YAQ_3AR; and (D) $YAQ_3P_{11}AR$.

9. "Fingerprint" region (NH-Cα) regions of CT-COSY spectra of polyQ and polyQ-polyP

peptides. CT-COSY spectra were measured at temperatures from 0 to 60 °C, at intervals of 5 °C,

to obtain $^3J_{NH-C\alpha}$. In all cases, peptides were in the mM concentration range, and solvent was 200

mM sodium phosphate, pH 7.00 with 0.1% NaN_3, w:v. The figure shows samples of CT-COSY

spectra measured at 0 °C for (A), R_3GQ_3GY; (B), $R_3GQ_3P_{11}GY$; (C), YAQ_3AR; and (D)

$YAQ_3P_{11}AR$.

10. Non-linear least squares fits of data from 1-D slices of CT-COSY spectra to an equation of

the difference between two Lorentzian functions. Examples shown are all for one Gln residue at

~ 0 °C for four peptides, (A), R_3GQ_3GY; (B), $R_3GQ_3P_{11}GY$; (C), YAQ_3AR; and (D)

$YAQ_3P_{11}AR$.

11.   Estimation of diffusion coefficients of R_3GQ_3GY and $R_3GQ_3P_{11}GY$, by comparison with a

protein standard, FN3s. These are the same data as shown in Figure 5, but without normalizing

the initial signal intensities, I_0. Data are shown for two peptides, (A), R_3GQ_3GY, and (B)

$R_3GQ_3P_{11}GY$, and for a protein standard, (C), FN3s, a small protein of known dimensions.

Points are experimental data; lines are fits to the equation of a monoexponential decay, i.e., I =

$I_0exp(-kt)$, where I = signal intensity, I_0 = initial signal intensity, and k is the rate constant. The

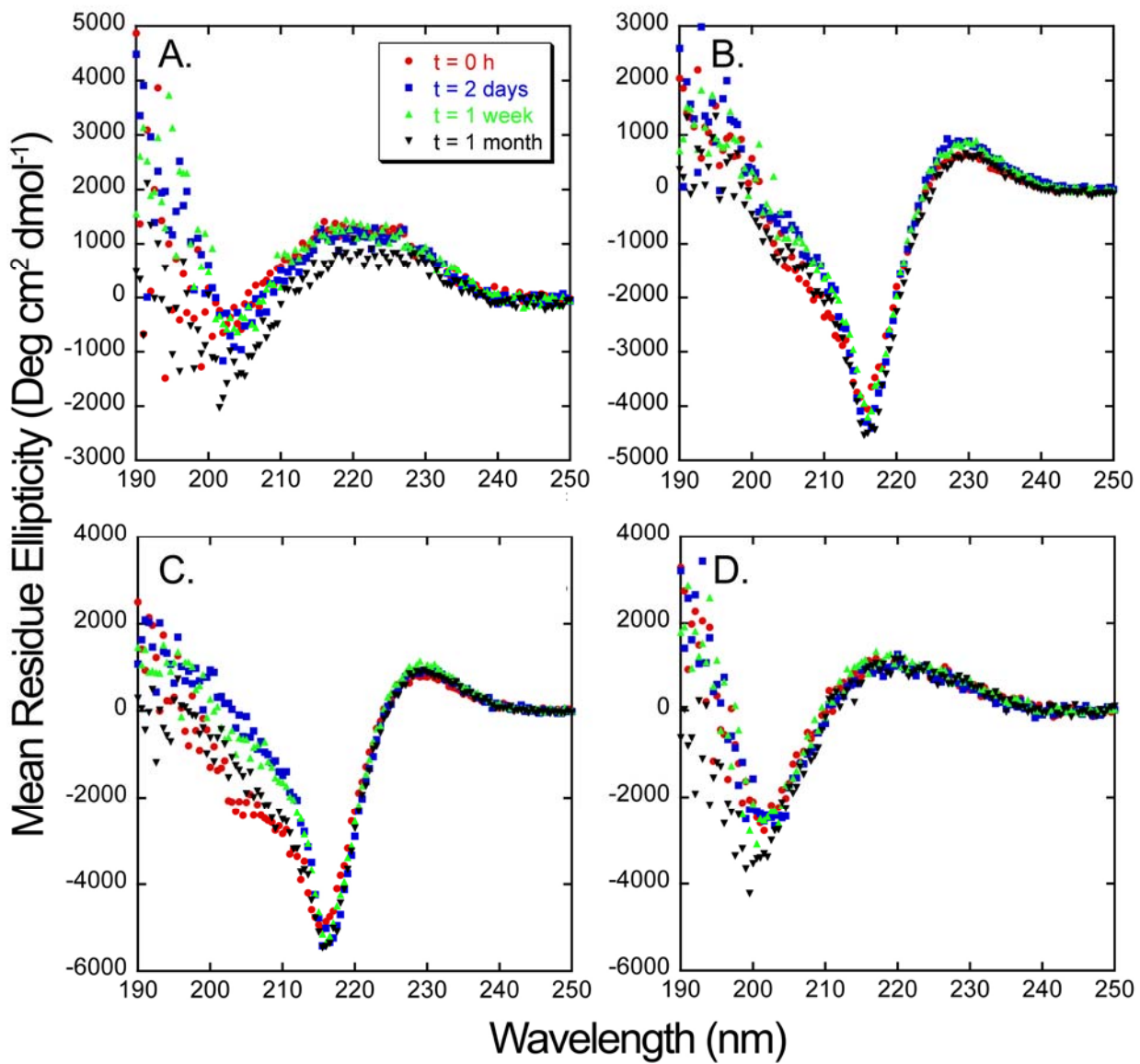units in the x-axis are derived from spin-lattice relaxation and are proportional to time.
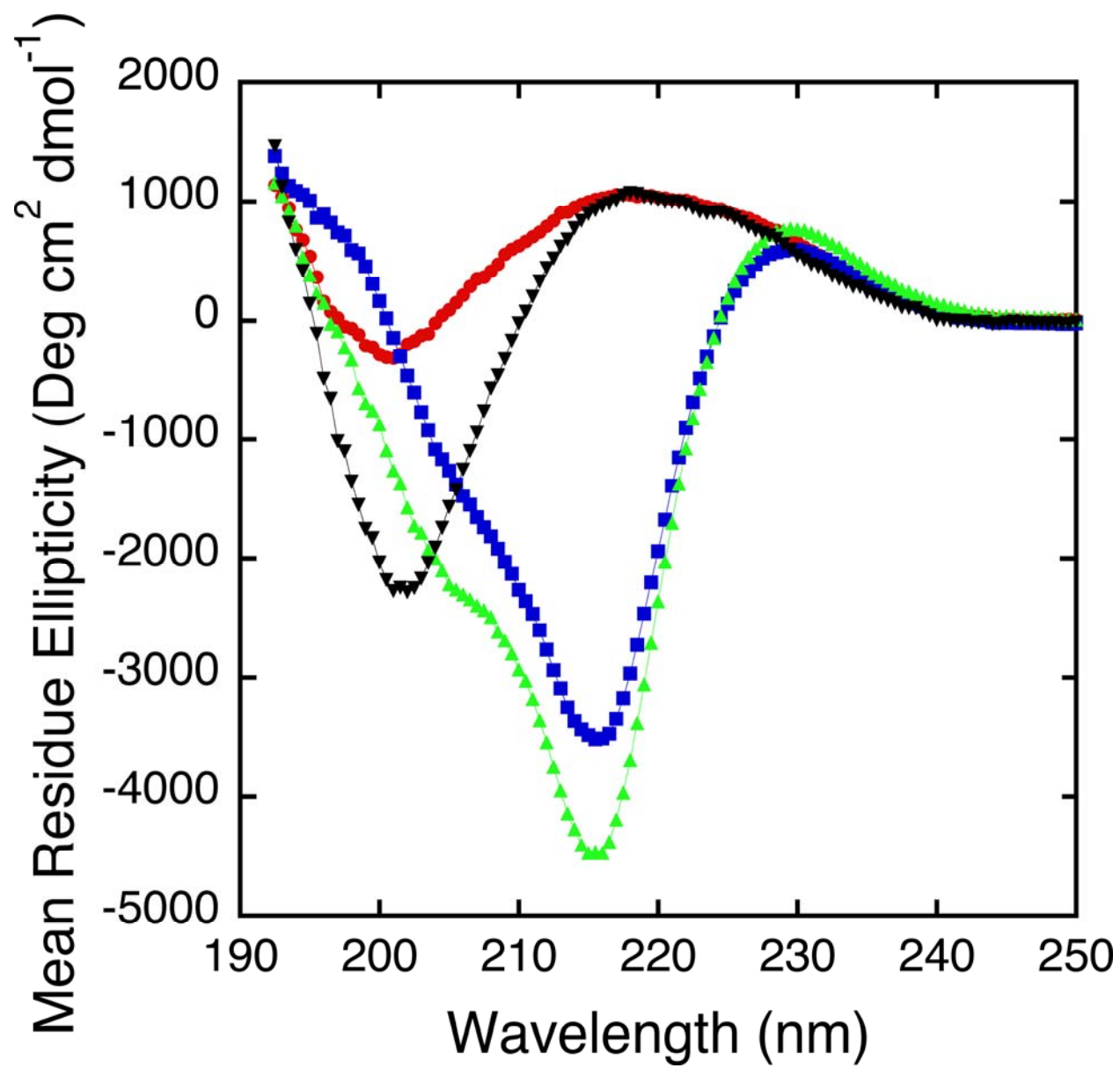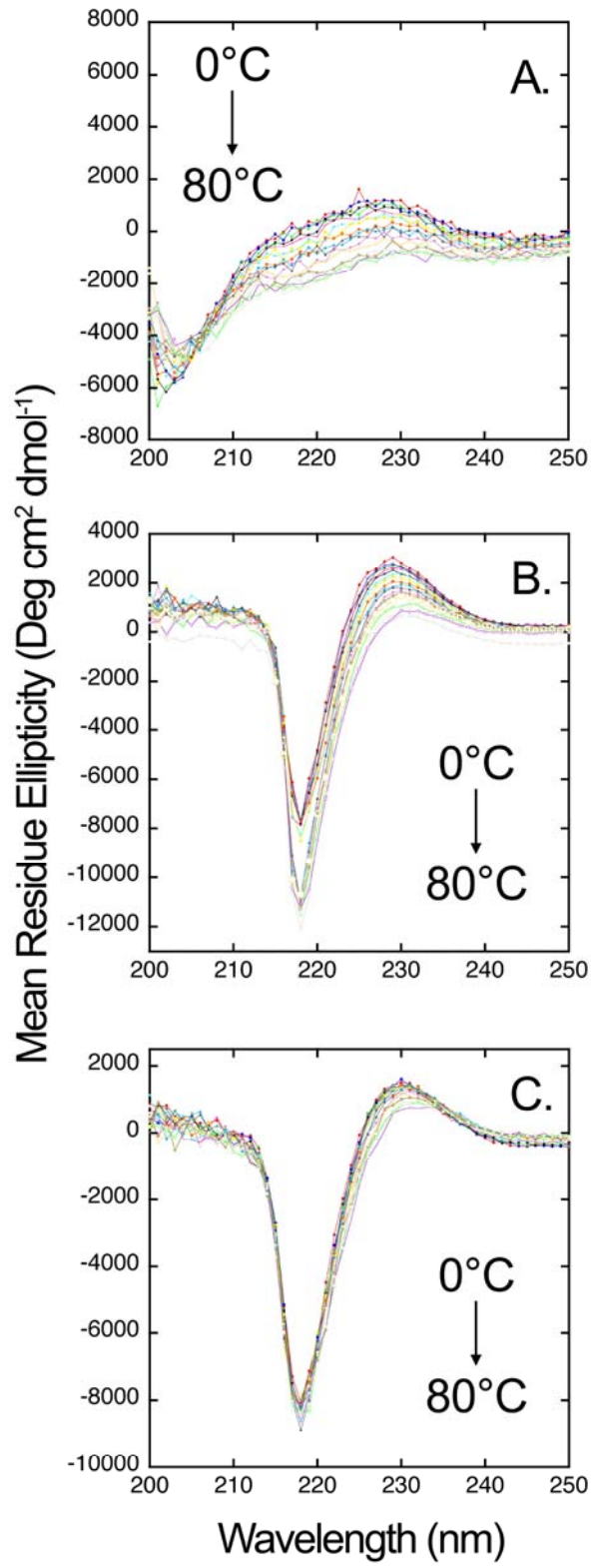
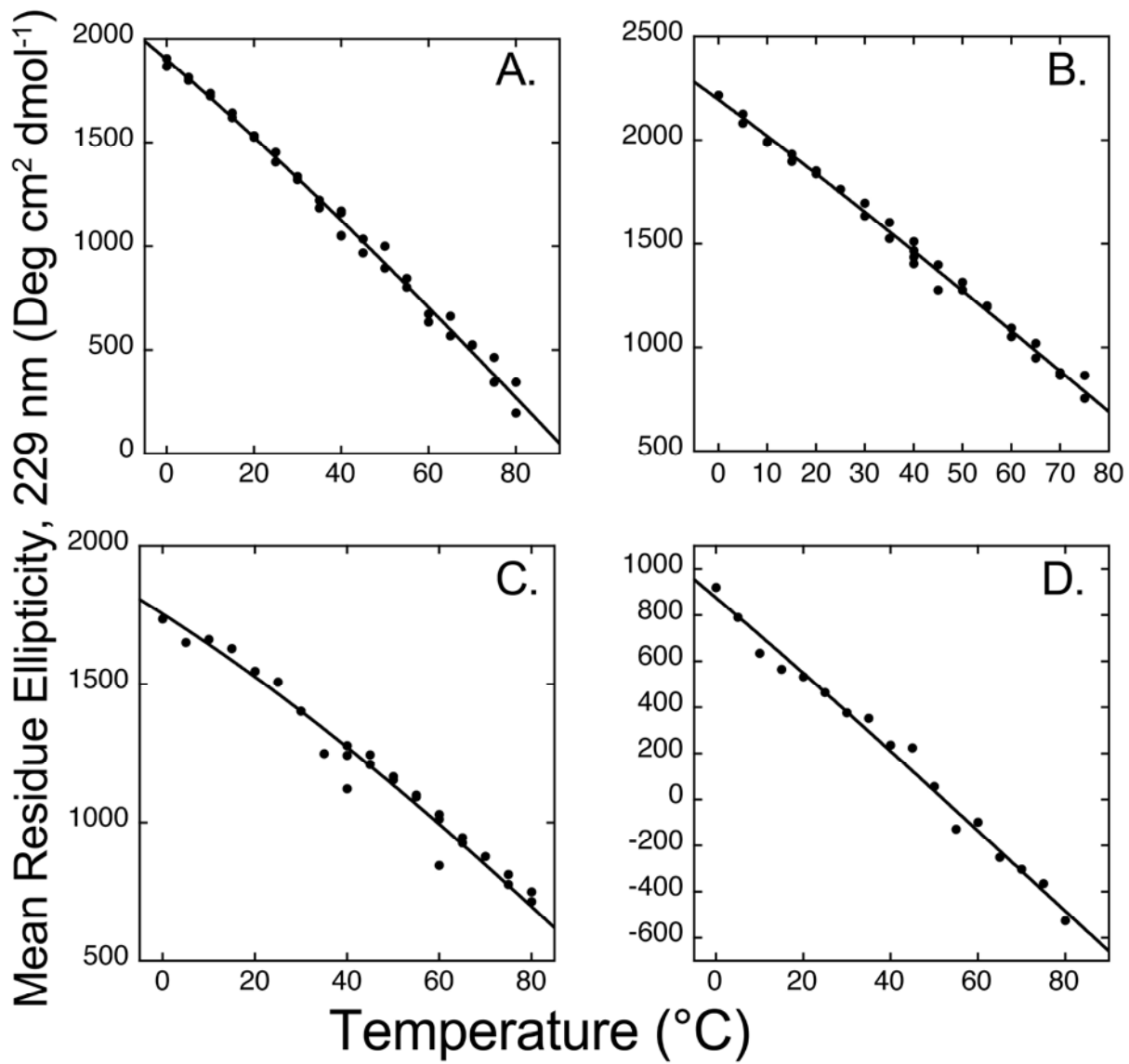Supplementary Figure 1
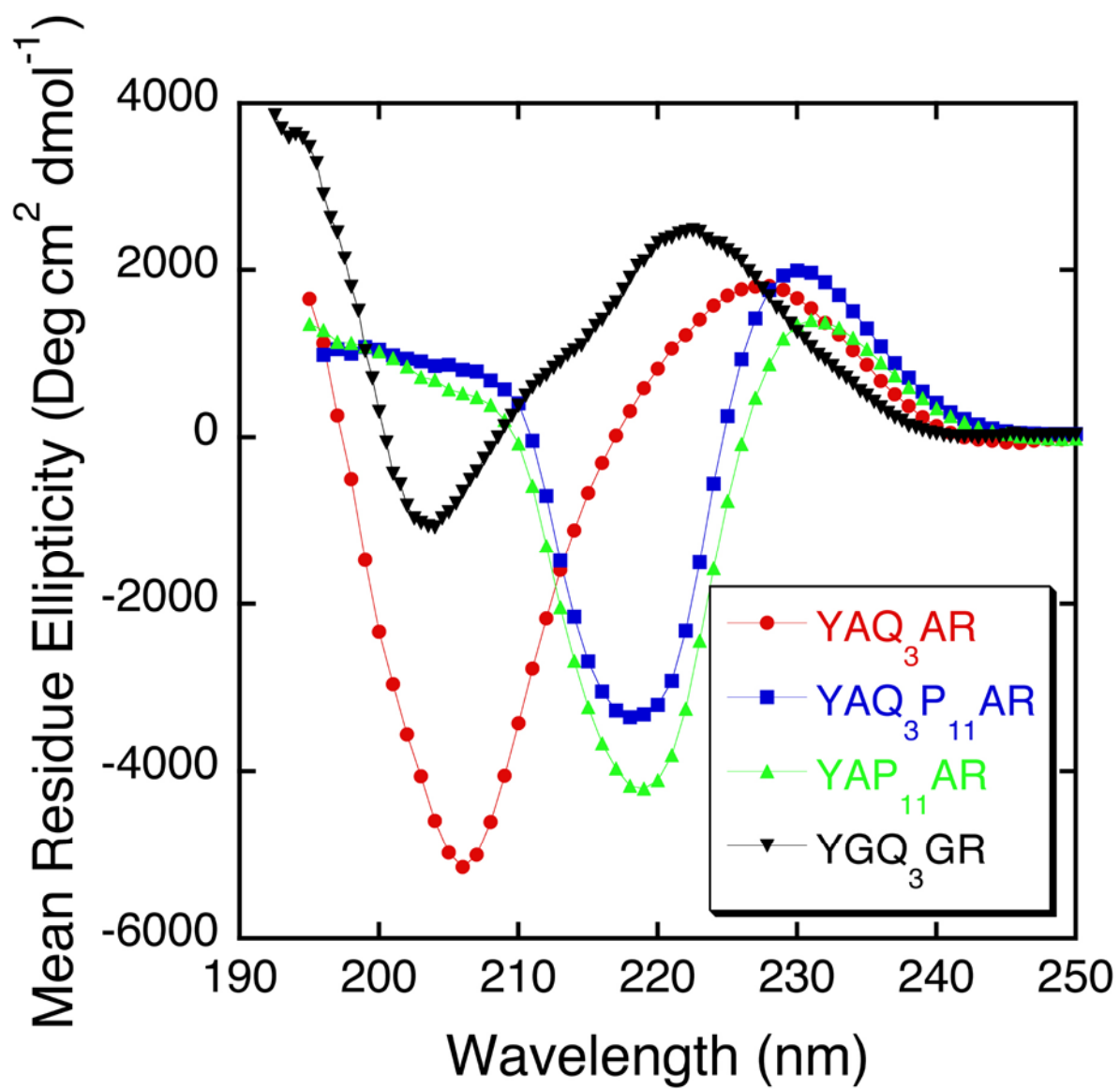
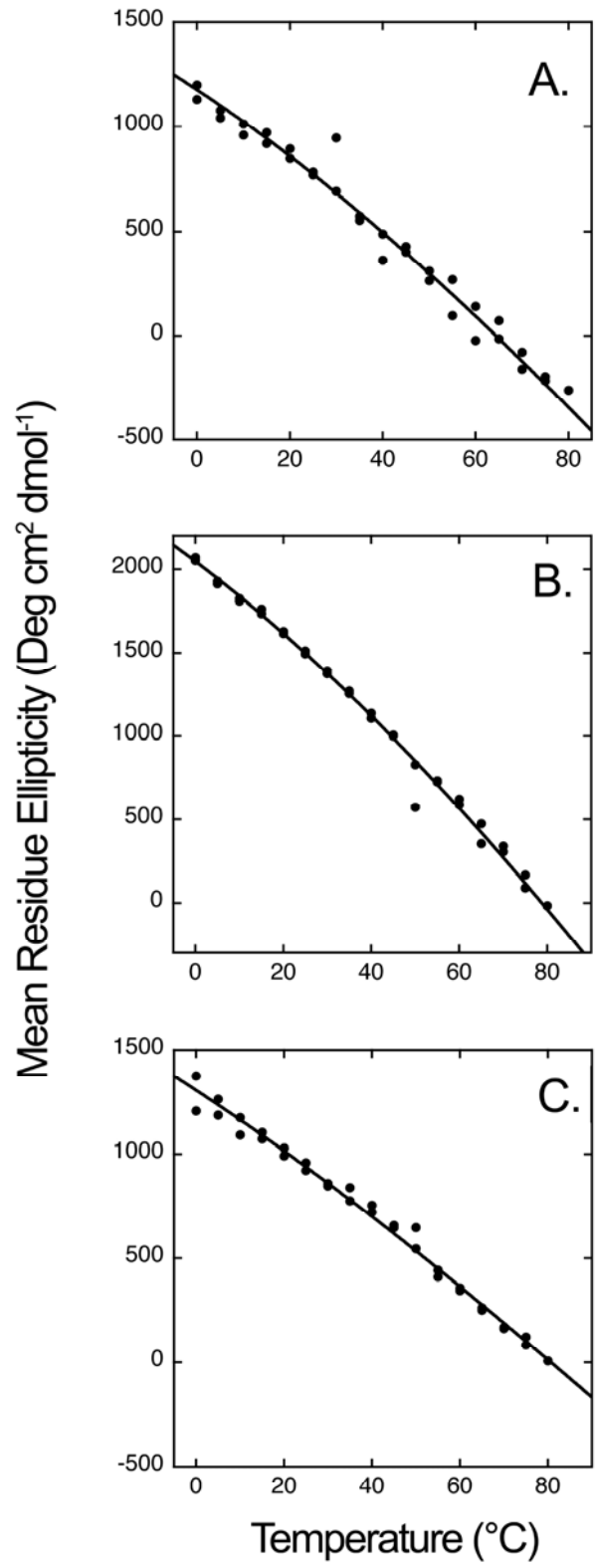Supplementary Figure 2
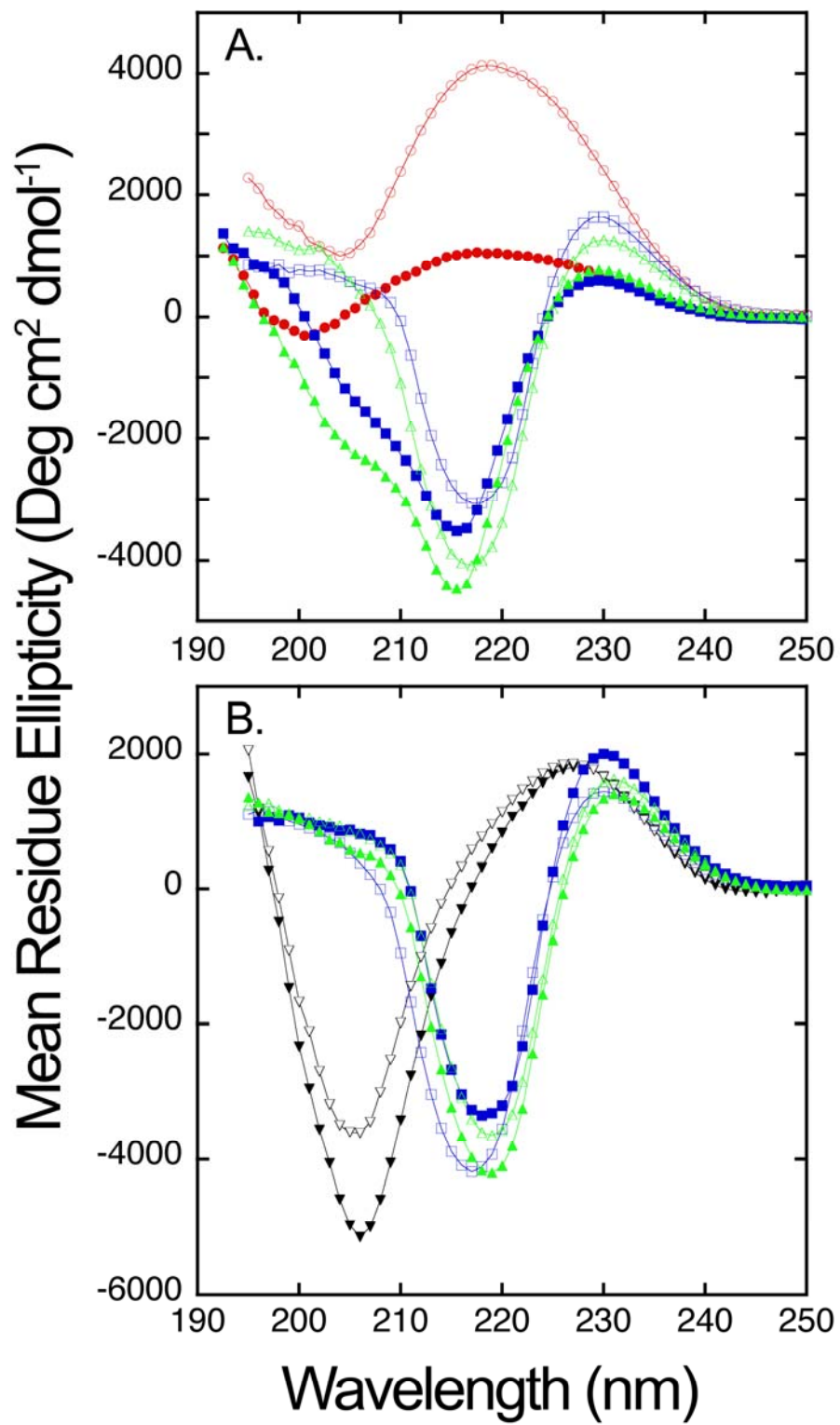
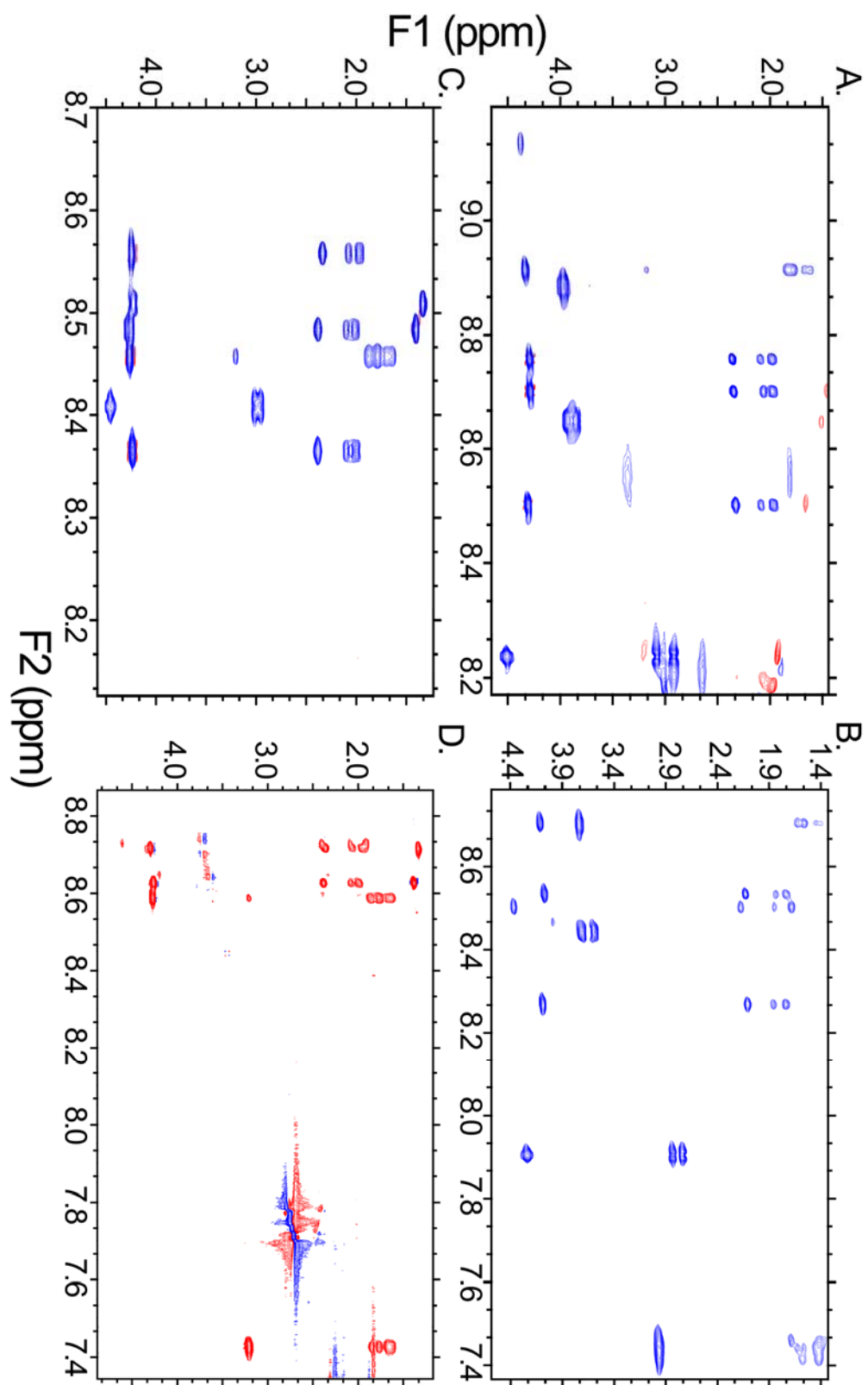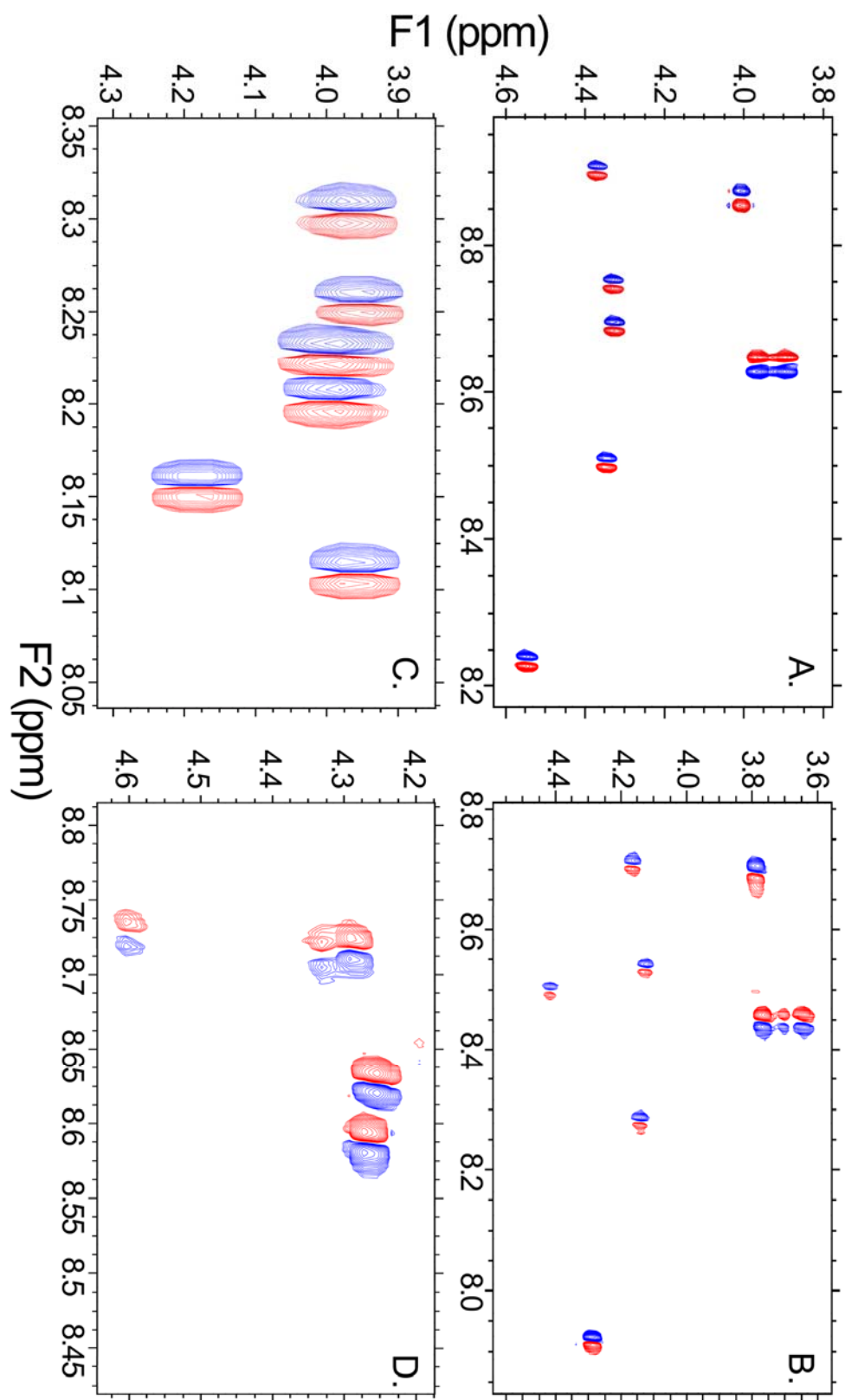Supplementary Figure 3

Supplementary Figure 4

Supplementary Figure 5

Supplementary Figure 6

S23

Supplementary Figure 7

S24
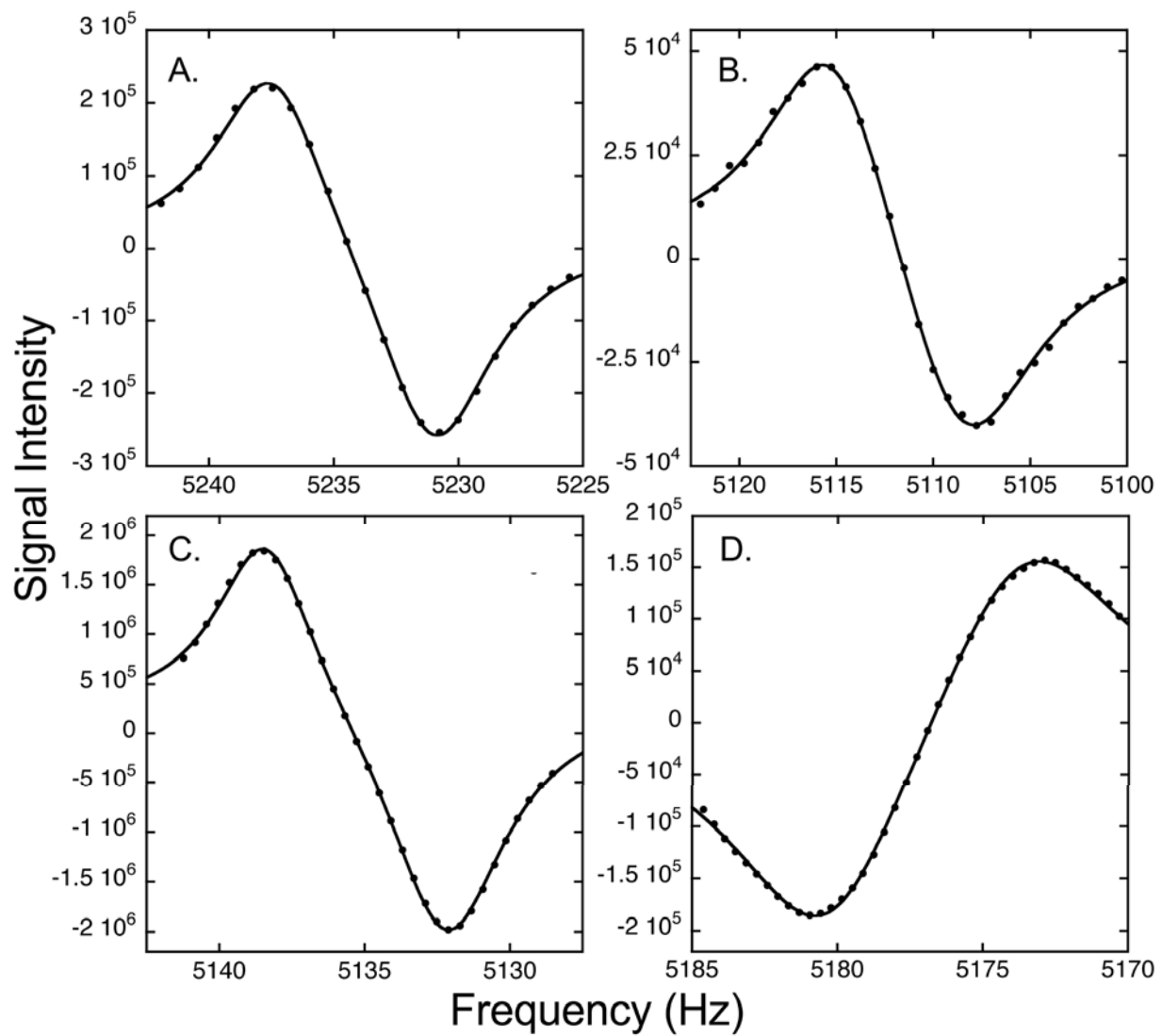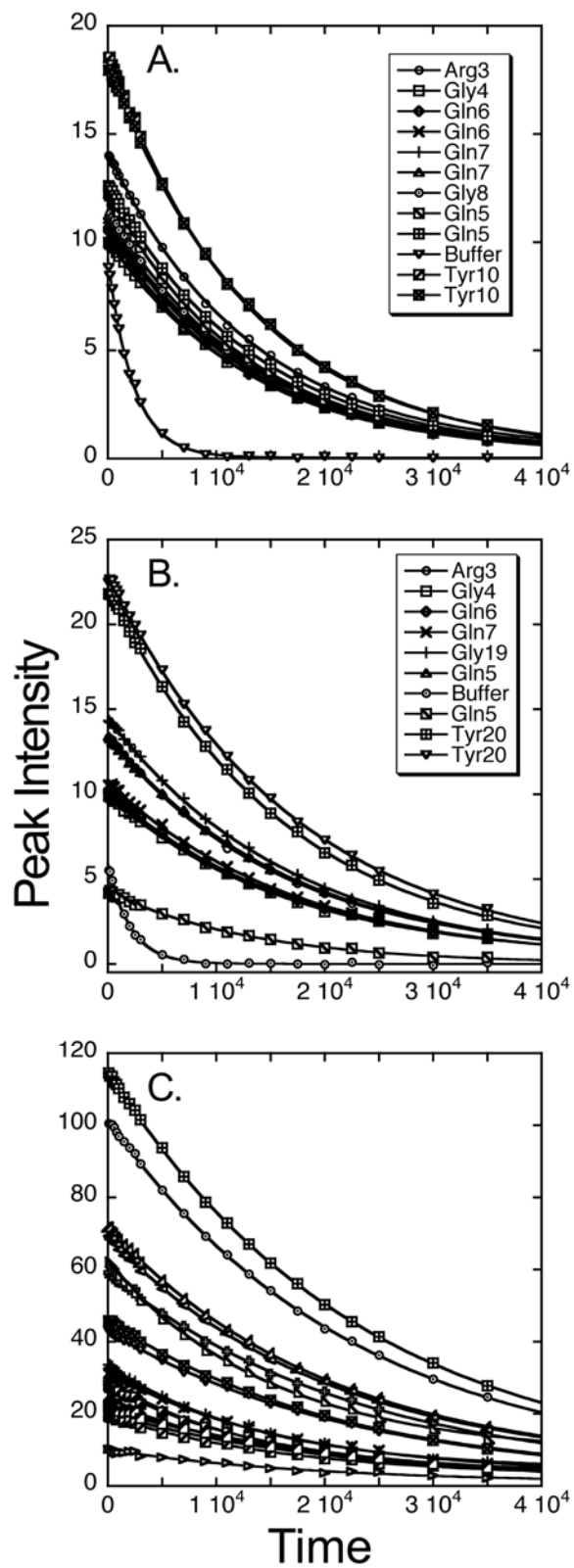
Supplementary Figure 8

Supplementary Figure 9

Supplementary Figure 10

Supplementary Figure 11